Cumulant analysis of the extended x-ray-absorption fine structure of β-AgI

G. Dalba and P. Fornasini
Dipartimento di Fisica, Università degli Studi di Trento, I-38050 Povo, Trento, Italy

F. Rocca
Centro di Fisica degli Stati Aggregati ed Impianto Ionico, del Consiglio Nazionale delle Ricerche e Istituto Trentino di Cultura, I-38050 Povo, Trento, Italy

(Received 1 June 1992; revised manuscript received 4 November 1992)

The extended x-ray-absorption fine structure (EXAFS) at the K edge of silver has been measured in β-AgI at different temperatures in the range T=23–410 K. Amplitude and phase of the first-shell EXAFS have been separately analyzed in terms of cumulant expansion within the photoelectron wave-vector range k=2.5–16.5 Å^{-1} taking the 23-K spectrum as reference. Tests on EXAFS simulated from excluded-volume-model distributions have been performed to check the convergence of the cumulant series and the correspondence between polynomial coefficients obtained from EXAFS analysis and exact cumulants. The cumulant series of the Ag–I distance distribution is convergent within the k and T ranges considered; below 300 K the polynomial coefficients are a good estimate of the exact cumulants; above 300 K the exact cumulants can be obtained by extrapolating the behavior of the polynomial coefficients below 300 K. The distributions of distances calculated from the cumulants are consistent with those obtained for β-AgI by other authors through a real-space analysis of EXAFS. The mean-square relative displacement is largely insensitive to anharmonicity as a consequence of the high degree of correlation of the motion of silver and iodine nearest neighbors.

I. INTRODUCTION

The determination of the local structure and dynamics in disordered solids can greatly benefit from the analysis of the extended x-ray-absorption fine structure (EXAFS). The development of a relatively simple interpretation of EXAFS (Ref. 1) in terms of interatomic distances and coordination numbers allowed its widespread application to many different physical systems.[2] This *standard* interpretation of EXAFS is based on the one-particle and single-scattering approximations (many-body effects being accounted for by phenomenological parameters). Moreover, only small Gaussian disorder is considered and the distribution of interatomic distances is completely characterized by its mean value and width: The so-called EXAFS *Debye-Waller factor* takes into account the *mean-square relative displacement* (MSRD) of absorber and backscatterer atoms.[3]

Standard EXAFS formula can lead to non-negligible errors in structural parameters when the distribution of interatomic distances differs from a narrow Gaussian one.[4,5] This situation typically arises when anharmonicity or anisotropy in thermal vibrations is non-negligible and in the presence of non-Gaussian static disorder. Even if the *real* distribution of interatomic distances is Gaussian, EXAFS samples an intrinsically asymmetric *effective* distribution.

The ability of recognizing and possibly measuring the deviation from a Gaussian distribution is necessary to check the applicability of standard EXAFS formula. For large deviations from Gaussian behavior, one is forced to formulate physical models for the distributions and to compare them with experimental EXAFS. The arbitrariness of models can be reduced if one is able to extract from EXAFS some model-independent parameters. These parameters can often give original information independently of a full knowledge of the distribution, as is the case of the MSRD, which reflects peculiar vibrational properties.

An increase of model-independent information from EXAFS can be achieved by analyzing data in terms of cumulants of the distance distribution.[6] The cumulants of order higher than 2 are zero for Gaussian distributions; their values measure then the deviation from a Gaussian shape.

Tranquada and Ingalls[7] utilized the cumulant approach to study the anharmonicity in CuBr. A more extensive exploration of strength and limitations of the cumulant method was done by Crozier, Rehr, and Ingalls.[8] These latter authors studied an exponentially skewed model distribution and showed that the convergence interval of its cumulant series can be quite small for large, although still physically meaningful, asymmetries; as a consequence, the first even cumulants obtained from EXAFS analysis were affected by exceedingly large errors. On the other hand, the polynomial coefficients best fitting amplitudes and phases of experimental EXAFS of CuBr allowed the same authors to reconstruct a distance distribution in reasonable agreement with that obtained through a real-space model-dependent analysis.

A widespread study of different physical systems is necessary to assess on general grounds the effectiveness of the cumulant analysis of EXAFS. The cumulant method relies on the ability of evaluating, from the EXAFS spec-

trum of an *a priori* unknown distribution of distances, the convergence properties of its cumulant series. This evaluation is necessary to estimate the accuracy of the polynomial coefficients obtained from EXAFS in reproducing the exact cumulants and in reconstructing the distribution of distances.

In this work we present the results of EXAFS measurements at the K edge of silver in β-AgI at different temperatures varying in the range 23–410 K. Silver iodide is particularly suited to study the strengths and limitations of the cumulant method. At atmospheric pressure and below 420 K, AgI has two crystalline modifications: the β and γ phases, with hcp wurtzite and fcc zinc-blende structure, respectively; β-AgI is considered the thermodynamically stable phase.[9] At 420 K, AgI undergoes a first-order transition to the superionic α phase. A strong anharmonicity has been revealed in β-AgI already at relatively low temperatures by x-ray diffraction (XRD) and neutron diffraction.[10–12] An EXAFS study of the silver-iodine correlation in AgI was performed by Boyce, Hayes, and Mikkelsen;[13] their interest was focused on the $\beta \rightarrow \alpha$ phase transition, which was described by an excluded-volume model. In this model the distribution of distances progressively deviates from a Gaussian shape when increasing the temperature, leading to the opening of conduction channels at 420 K. The model was consistent with measurements made on the β phase at 300 and 371 K.[14]

More recently Dalba *et al.* studied the MSRD of the I–Ag and I–I distances in β and γ-AgI obtained from I L_3 EXAFS in the temperature range 11–300 K.[15,16] The use of the standard data reduction procedure was justified by the shortness of the EXAFS signal at the I L_3 edge. The temperature dependence of the MSRD's was found consistent with the harmonic approximation. A better understanding of the effects of anharmonicity on the MSRD of β-AgI could be gained by a more refined cumulant analysis.

In the present study of Ag K EXAFS, only the first coordination shell of silver is considered; the possible multiple-scattering paths do not interfere with the first-shell EXAFS signal, and so we rely on the single-scattering approximation. The analysis is carried on by separately comparing phases and amplitudes of EXAFS spectra at various temperatures with those of the 23-K reference spectrum, so that backscattering amplitude, total phase shift, and anelastic terms cancel out. The result of the analysis is the temperature dependence of the polynomial coefficients best fitting phase and amplitude of EXAFS. To test the reliability of these polynomial coefficients in estimating the exact cumulants, we considered the distance distribution of the excluded-volume model with the parameters best fitting the EXAFS at 300 and 371 K (Ref. 14) and submitted it to the same procedure of EXAFS analysis done on the experimental data. A preliminary short account of this work has been given elsewhere.[17]

This paper is organized as follows. In Sec. II we review some concepts of the cumulant method which are relevant for our work. Section III is dedicated to experimental details on sample preparation and EXAFS measurements. In Sec. IV a detailed account of the data analysis procedure is given. In Sec. V the tests on model distributions are presented. In Sec. VI the temperature dependence of the first four cumulants and the distributions of distances obtained from cumulants are discussed and compared with previous results from EXAFS and other techniques. Section VI is dedicated to conclusions.

II. CUMULANT EXPANSION OF EXAFS

Let $\rho(r)$ be the *real* distribution of distances between the absorber atom and one atom of a given coordination shell. Within the single-electron, single-scattering, and plane-wave approximations, the EXAFS of the sth coordination shell is expressed as[6,8]

$$\chi_s(k) = \frac{S_0^2}{k} N_s \operatorname{Im}\left\{ f_s(k,\pi)\, e^{2i\delta_1} \int_0^\infty P(r,\lambda)\, e^{2ikr}\, dr \right\}, \tag{1}$$

where k is the photoelectron wave vector, N_s the coordination number, $f_s(k,\pi)$ the complex backscattering amplitude, and δ_1 the central atom phase shift. S_0^2 and λ take into account intrinsic and extrinsic anelastic effects, respectively. $P(r,\lambda)$ is the *effective* distribution of distances,

$$P(r,\lambda) = \rho(r)\, \frac{e^{-2r/\lambda}}{r^2}. \tag{2}$$

The possible symmetry of the *real* distribution $\rho(r)$ is not preserved by the *effective* distribution $P(r,\lambda)$. In the following we will neglect the k dependence of the mean free path λ; this approximation is generally acceptable for an EXAFS analysis based on the comparison with a reference compound when, as in our case (see below), the same sample at different temperatures is used as both an unknown and as a reference.[6]

The integral on the right-hand side of Eq. (1) is the characteristic function of the effective distribution $P(r,\lambda)$. The knowledge of an EXAFS signal does not allow a complete recovering of the characteristic function. Apart from difficulties connected with backscattering amplitudes, phase shifts, and anelastic terms, which can often be overcome by a suitable choice of reference compounds, the main drawback is the limited k range of the EXAFS signal. The cumulant method can allow to reconstruct the low k missing part of the EXAFS signal with reasonable accuracy.

The logarithm of the characteristic function can be developed in Mac Laurin series around $k = 0$:

$$\ln \int_0^\infty P(r,\lambda)\, e^{2ikr}\, dr = C_0 + \sum_{n=1}^{\infty} \frac{(2ik)^n}{n!}\, C_n. \tag{3}$$

The C_n coefficients are called *cumulants* or *seminvariants* of the distribution $P(r,\lambda)$ and are connected to the moments by simple relations.[18,19] C_0 depends on the normalization of $P(r,\lambda)$; C_1 and C_2 correspond to mean value $\langle r \rangle$ and variance $\langle (r - \langle r \rangle)^2 \rangle$ of $P(r,\lambda)$, respectively. For Gaussian distributions the cumulants C_n with $n > 2$

are zero. The convergence interval of the cumulant series depends on the shape of $P(r,\lambda)$.

By substituting Eq. (3) into Eq. (1), the EXAFS of the sth coordination shell can be expressed, within the convergence interval, through the cumulant series of the effective distribution $P(r,\lambda)$. Even and odd cumulants determine amplitude and phase of the EXAFS signal, respectively.

The cumulants C_n can in principle be obtained by comparison with the EXAFS of a reference compound. The difference between the EXAFS phases is

$$\Phi_s(k)-\Phi_r(k)=2k\Delta C_1-\tfrac{4}{3}k^3\Delta C_3+\tfrac{8}{15}k^5\Delta C_5+\cdots, \tag{4}$$

while the logarithm of the amplitude ratio is

$$\ln\frac{A_s(k)}{A_r(k)}=\ln\frac{N_s}{N_r}+\Delta C_0-2k^2\Delta C_2+\frac{2}{3}k^4\Delta C_4-\frac{4}{45}k^6\Delta C_6+\cdots, \tag{5}$$

where $\Delta C_i=C_i^s-C_i^r$, s labeling the unknown sample, r the reference. For not too large distributions one can approximate $\exp(C_0)=\exp(-2C_1/\lambda)/C_1^2$, so that

$$\Delta C_0=-2\frac{C_1^s-C_1^r}{\lambda}-2\left[\ln C_1^s-\ln C_1^r\right]; \tag{6}$$

this term, often negligible, can easily be estimated from a rough knowledge of interatomic distance and mean free path.

Phase differences and logarithms of amplitude ratios can reasonably be fitted by finite polynomials of relatively low degree: One obtains the ratio of coordination numbers N_s/N_r and the variation $\Delta\tilde{C}_i$ of a limited number of polynomial coefficients. The polynomial coefficients $\tilde{C}_i$ are a good approximation to the exact cumulants only if the series on the right-hand sides of Eqs. (4) and (5) are rapidly convergent.

The cumulants of the *real* distribution differ from those of the effective distribution by a relative error of order C_2/C_1^2, which is generally negligible for cumulants of order higher than 1.[6] The mean value R_s of the real distribution can be obtained from C_1 through

$$R_s=C_1+\frac{2C_2}{C_1}\left(1+\frac{C_1}{\lambda}\right). \tag{7}$$

If the *real* distribution $\rho(r)$ is sufficiently narrow, the corresponding *effective* distribution $P(r,\lambda)$ can be approximated by a Gaussian one with mean and width equal to those of the real distribution; the cumulants of order higher than 2 can then be neglected and the standard EXAFS formula utilized: The width σ of the distribution is accounted for by the EXAFS Debye-Waller factor $\exp(-2\sigma^2k^2)$.[2]

III. EXPERIMENTAL DETAILS

To prepare the β-AgI sample for EXAFS measurements, we started from a high purity AgI powder (purchased from C. Erba, Italy), which was a mixture of β and γ phases, and added it up to saturation to a concentrated KI:H_2O solution. The slowly deposited powder, washed in methyl alcohol, was characterized by XRD as a high purity hcp β phase. To get homogeneous samples of uniform thickness, as required by x-ray-absorption measurements in transmission mode, the powder was dispersed in alcohol and slowly deposited on polytetrafluoroethylene membranes. Samples with absorption discontinuity $\Delta\mu x\simeq 0.9$ at the silver K edge were so obtained. More details on preparation and characterization of samples have been given elsewhere.[20]

EXAFS measurements were performed at the beam line D42 (EXAFS 1) of the storage ring DCI at LURE (Laboratoire pour l'Utilisation du Rayonnement Electromagnétique), Orsay, France. The electron-beam energy was 1.85 GeV and the maximum stored current 300 mA. The monochromator was a channel-cut silicon crystal, with reflecting faces (331).

Absorption spectra were recorded in transmission mode, utilizing as detectors two ion chambers fluxed with argon gas at atmospheric pressure. A temperature range extending from 23 to 410 K was systematically explored. Temperature control was achieved, below 300 K, by a helium gas flow cryostat containing an heating electric resistor; above 300 K an oven was utilized with a programmable controller. The temperature was monitored by thermocouples; the accuracy was estimated about ± 2 K. Two separate experimental runs were done: from 23 to 300 K and at 23 and 75 and from 200 to 410 K, respectively. The two measurement sets were in good agreement at the temperatures of overlap.

Standard energy calibration at the K edge of metallic silver (25 517 eV) was made before each measurement run. The average acquisition step was 3 eV with a maximum recording time of 10 s per step. The energy resolution was $\Delta E\simeq 9.5$ eV, mainly determined by the divergence of the photon beam (the vertical dimension of the beam was 1 mm at the sample). The energy width of the Ag K excited state is about 7.5 eV. The relatively high resolution ΔE was a compromise between contrasting requirements of high flux and high resolving power, and allowed us to collect a meaningful EXAFS signal at energies as high as 1 keV above the edge even at 410 K in a reasonable time. Lengeler and Eisenberger[21] have shown that the damping of EXAFS due to the finite-energy resolution can be taken into account by an exponential factor whose argument varies as $-1/k^2$ and depends on temperature only through the interatomic distance. Our EXAFS analysis is based on phase differences and amplitude ratios: All temperature-independent terms cancel, including the correcting factor of Lengeler and Eisenberger, so long as the distance variations are small.

IV. EXAFS DATA ANALYSIS

The spectra taken at different temperatures were compared in the edge region to get a fine relative calibration of the energy scales. The photoelectron wave vector $k=[2m(\hbar\omega-E_0)]^{1/2}/\hbar$ was then calculated from the photon energy $\hbar\omega$ by conventionally setting E_0 in correspondence with the maximum of the first derivative of

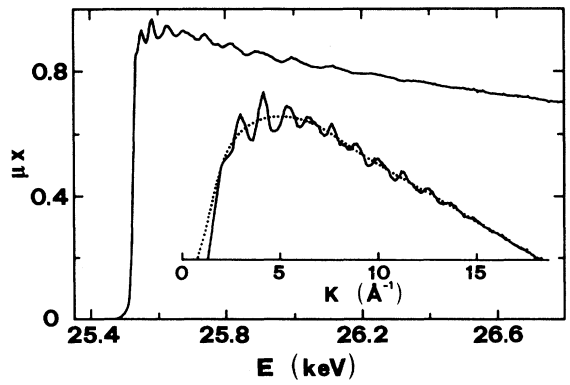

FIG. 1. X-ray-absorption spectrum at the Ag K edge of β-AgI measured at 23 K. In the inset an enlarged view is plotted as a function of photoelectron wave vector: The dotted line is a polynomial spline best fitting the average behavior of EXAFS oscillations.

each spectrum. The EXAFS $\chi(k)$ was obtained from the absorption coefficient $\mu(k)$ as

$$\chi(k) = \frac{\mu(k) - \mu_1(k)}{\mu_0(k)}; \tag{8}$$

$\mu_1(k)$ was a spline curve best fitting the average behavior of $\mu(k)$ above the absorption edge (Fig. 1) and optimized by minimizing the spurious structures below about 2 Å in the Fourier transform; $\mu_0(k)$ was a smooth function with a Victoreen-like slope and absolute values normalized to the experimental absorption jump.

The EXAFS signal is shown in Fig. 2 for the two temperatures 23 and 390 K. The low-frequency EXAFS oscillations underlying the high-frequency noise revealed meaningful, after Fourier filtering, for $k \leq 16.5$ Å^{-1} even at the highest temperatures.

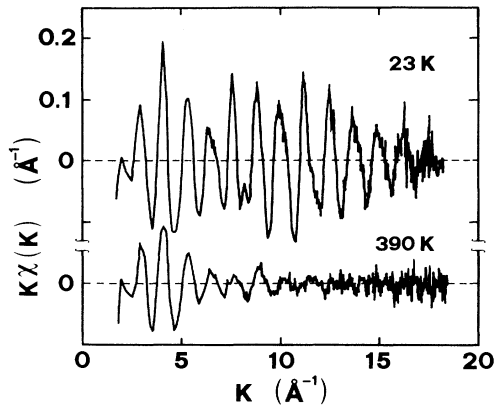

FIG. 2. EXAFS oscillations $k\chi(k)$ at the Ag K edge of β-AgI at 23 K (top) and 390 K (bottom).

A. Fourier filtering

The modulus of Fourier transform (FT) of $k^2\chi(k)$ is shown in Fig. 3 for selected temperatures. The first-shell peak (4 iodine atoms at about 2.81 Å) progressively decreases and modifies its shape when temperature increases. The second-shell peak (12 silver atoms at about 4.59 Å) is more quickly damped and is indistinguishable from noise already at 50 K. A different situation was found at the edge L_3 of iodine, where the second-shell signal (distances I–I) was well distinguishable at least up to 300 K.[15,16] The different behavior of the second-shell signal in the Ag K EXAFS with respect to the I L_3 EXAFS is probably due to a joint effect of the short lifetime of the excited K state of silver and of the relatively large amplitude of thermal vibrations of the Ag–Ag couple.

The contribution of the first coordination shell was singled out and backtransformed to k space. The real part of the backtransformed signal corresponds to the Fourier-filtered EXAFS and is shown in Fig. 4(a) for 23 and 390 K. From the real and imaginary parts of the filtered signal the total phase $\Phi(k)$ and amplitude $A(k)$ of EXAFS were obtained [Figs. 4(b) and 4(c)]. At $k \simeq 6.5$ Å^{-1} the amplitude is characterized by a minimum and the phase by an inflection, reflecting the resonant behavior of the complex backscattering amplitude of iodine (a similar be-

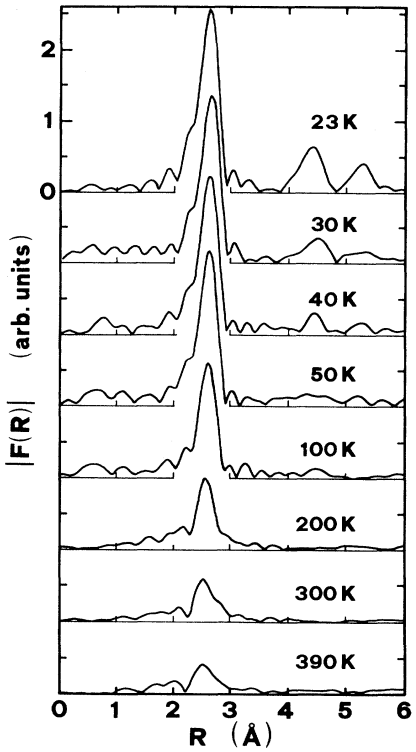

FIG. 3. Fourier transforms (FT's) of β-AgI EXAFS at different temperatures. The EXAFS signal in the k interval 2.5–16.5 Å^{-1} was weighted by k^2 and convoluted with a 20% Hanning window.

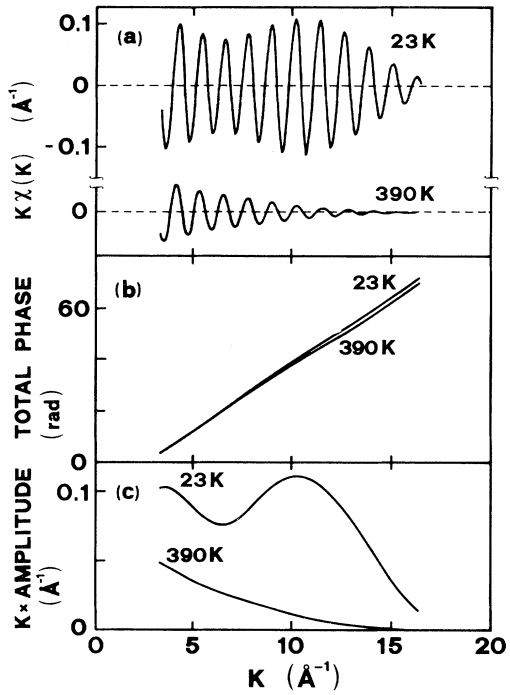

FIG. 4. Fourier-filtered EXAFS of the first coordination shell of silver in β-AgI at 23 and 390 K. From top: (a) $k\chi(k)$ signals, (b) their total phases, and (c) amplitudes.

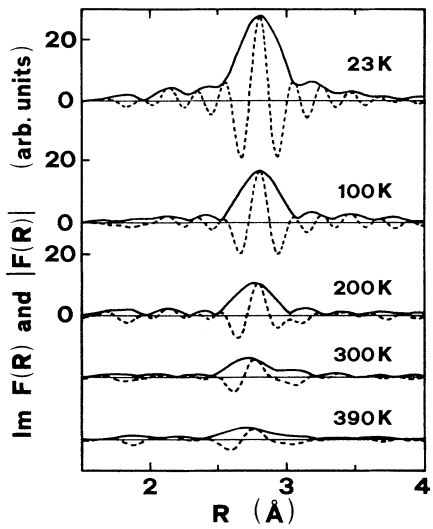

FIG. 5. FT's of β-AgI EXAFS at different temperatures, calculated after dividing the $\chi(k)$ signal by amplitude and exponential of total phase shift of the 23 K spectrum. The signal was weighted by k^2 and convoluted with a 20% Hanning window in the k interval 2.5–16.5 Å^{-1}. Dashed lines are imaginary parts; continuous lines are moduli of FT's.

havior was found at $\simeq 6$ Å^{-1} for the I L_3 EXAFS, where the backscatterer was silver[15]).

To reduce the uncertainties in phase and amplitude analysis arising from the resonant behavior at 6.5 Å^{-1}, we repeated the FT of the EXAFS signals after phase-shift and amplitude removal, following the method first suggested by Lee and Beni.[22] To this purpose, we used the phase shift and amplitude extracted from the 23-K reference EXAFS: At this temperature the distribution of Ag–I distances was supposed perfectly Gaussian and standard formula applicable (the soundness of this hypothesis was verified *a posteriori*, see Sec. VI); the experimental 23-K amplitude contains the still unknown Debye-Waller factor.

The FT was done over all the measured k range 2.5–16.5 Å^{-1}; k^2 weighting and 20% Hanning window were selected, after an exhaustive trial procedure, as those giving a reasonably good isolation of the first-shell peak at all temperatures. Imaginary parts and moduli of FT are shown in Fig. 5 for some temperatures. As expected, the first-shell peak in the 23-K spectrum is symmetric with respect to its mean value, corresponding now to the crystallographic Ag–I distance; the imaginary part is also symmetric and its maximum corresponds to that of the modulus. When temperature is raised the first-shell peak shifts towards shorter distances, becoming more and more asymmetric, and a growing mismatch is noticed between the maxima of modulus and imaginary part. This behavior monitors the progressive departure of the effective distribution sampled by EXAFS from symmetry.[8]

The first-shell peaks were isolated by asymmetric Hanning windows specifically tailored to the peak shapes (Fig. 6) and backtransformed to k space. This procedure gave a smooth behavior of phase differences and amplitude ratios, at the expenses of a non-negligible uncertainty in the phase at low k values (typically below 8 Å^{-1}). The alternative inclusion of the first sidelobes of the peak was also attempted: An apparently more reasonable behavior of low k phases was obtained, but fictitious structures appeared in both phases and amplitudes; tests performed on model distributions (Sec. V) showed that the inclusion of sidelobes produced less reliable results.

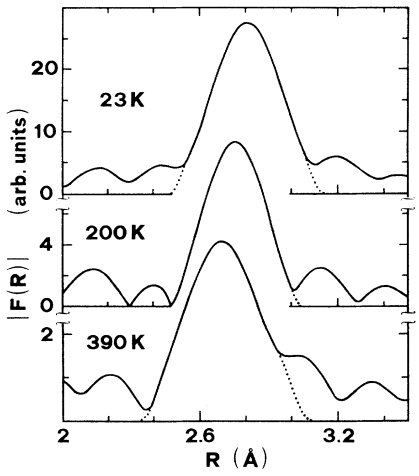

FIG. 6. Moduli of FT's of β-AgI EXAFS at 23, 200, and 390 K (solid lines). The dotted lines show the effect of the asymmetric Hanning windows utilized to isolate and back transform the central peak.

B. Phase and amplitude analysis

Phase differences $\Phi(T) - \Phi(23\ \text{K})$ of the first-shell EXAFS signals are plotted in Fig. 7 (solid lines) for selected temperatures. The deviation from linearity, which is the fingerprint of asymmetry in the effective distribution, roughly grows with temperature. The analysis of phase differences was done through Eq. (4) truncated at the third-order term. The polynomial coefficients $\Delta\tilde{C}_1$ and $\Delta\tilde{C}_3$ were determined by a best fit to the experimental curves in the k range 8–16 Å^{-1} (dashed lines in Fig. 7). The region below 8 Å^{-1} was considered less reliable in view of the sensitivity to the Fourier back-transform window. Moreover, the low resolving power and relatively large acquisition step reduce the accuracy of the EXAFS phase particularly at low k values and increase the uncertainty in the determination of the edge position E_0.

The phase difference curves could be made apparently more reasonable in the low k region (e.g., avoiding the crossing of the zero axis) by varying the E_0 values of the sample with respect to the model; ΔE_0 values as high as 4 eV were, however, required at 410 K. This procedure was rejected since no physical explanation was found for such large ΔE_0 values. ΔE_0 was *a priori* fixed to zero throughout all the analysis. The soundness of this choice was confirmed by tests on model distributions (Sec. V).

Equation (4) is strictly valid only if k refers to the true E_0 value. Let us here indicate by E_0' the energy at the maximum of the first derivative, and by k' the corresponding wave vector, and let be $\delta E_0 = E_0' - E_0$. Equation (4) should be modified, to a first approximation, to[8]

$$\Delta\Phi = (2\Delta C_1 - 2a\Delta C_3 \delta E_0)k' - \frac{4}{3}\Delta C_3 k'^3 + \frac{a\delta E_0}{k'}\Delta C_1,$$

where $a = \hbar/2m$. However, if the phase analysis is limited to $k' \geq 8$ Å^{-1} and for $\delta E_0 \leq 10$ eV, the additive terms are in our case negligible.

Logarithms of the amplitude ratios, $\ln A(T)/A(23\ \text{K})$, are plotted as a function of k^2 in Fig. 8 (solid lines) for some temperatures. Their analysis was performed through Eq. (5) truncated at the fourth-order term. Unlike phase analysis, amplitude analysis was insensitive to the ΔE_0 value, which was anyway set equal to zero. The polynomial coefficients $\Delta\tilde{C}_2$ and $\Delta\tilde{C}_4$ were determined by a best fit to the experimental curves in the k range 5–16.5 Å^{-1}. The ratio N_s/N_r was fixed to 1. ΔC_0 was calculated through Eq. (6) using the $\tilde{C}_1$ values obtained from phase analysis and a mean free path $\lambda \simeq 4$ Å, as calculated for AgI in the EXAFS region utilizing the imaginary part of an Hedin–Lundqvist potential.[20,23] Neglecting the contribution of ΔC_0 in Eq. (5) would lead to underestimating $\Delta\tilde{C}_2$ and $\Delta\tilde{C}_4$ at the highest temperatures by at most 3% and 5%, respectively. The choice of the λ value will be discussed in Sec. V; λ values reasonably larger than 4 Å would anyway produce effects smaller than the uncertainty of data analysis.

C. Results: polynomial coefficients

The analysis of phase differences and amplitude ratios gave four parameters at each temperature, say, the differences in polynomial coefficients $\Delta\tilde{C}_i = \tilde{C}_i(T) - \tilde{C}_i(23$

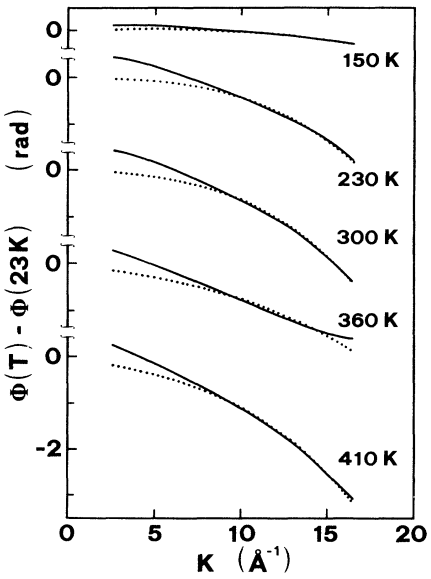

FIG. 7. First-shell EXAFS in β-AgI: difference between phases at different temperatures and at 23 K (solid lines). The dotted lines are polynomials, Eq. (4) truncated at the third-order term, best fitting the experimental curves in the k range 8–16 Å^{-1}.

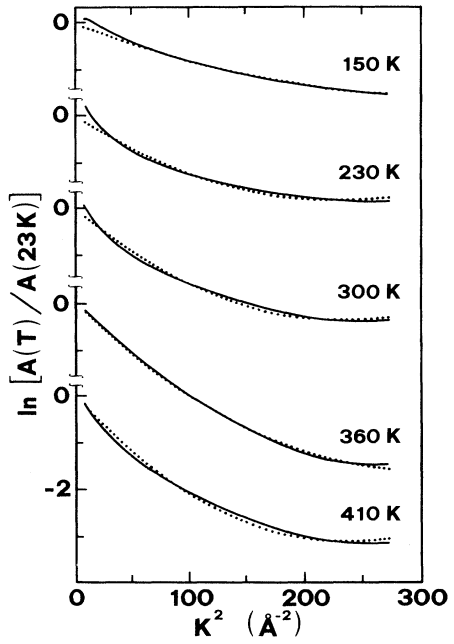

FIG. 8. First-shell EXAFS in β-AgI: logarithm of the ratio of EXAFS amplitudes at different temperatures and at 23 K (solid lines). The dotted lines are polynomials, Eq. (5) truncated at the fourth order term, best fitting the experimental curves in the k range 5–16.5 Å^{-1}. The coordination number was fixed to 4.

K), i=1,4. These parameters are shown in Fig. 9 (solid circles) as a function of temperature. By assuming a Gaussian distribution at 23 K, the absolute values $\tilde{C}_3$ and $\tilde{C}_4$ are directly obtained from EXAFS analysis. The absolute values, obtained as explained below, are plotted in Fig. 9 also for $\tilde{C}_2$. The anharmonicity of β-AgI is qualitatively monitored by the growth of $\tilde{C}_3$ and $\tilde{C}_4$ with temperature.

To estimate the uncertainty due to the data reduction procedure we repeated the analysis varying some of the most relevant parameters, for example, shortening the k fitting range of phase differences and amplitude ratios. The vertical bars in Fig. 9 represent the standard deviation of the results obtained. The different procedures utilized were not equivalent; the tests on model distributions (Sec. V) showed that the procedure giving the solid circles in Fig. 9 should be considered the most reliable. In the following we will then refer to these values rather than to statistical averages over all the attempted procedures.

Our main concern is now to determine whether the polynomial coefficients obtained from EXAFS are a reasonably good estimate of the cumulants of the effective distributions. The distributions and the convergence properties of their cumulant series are *a priori* unknown. We assume, however, a Gaussian distribution at 23 K and expect a fast convergence of the cumulant series for sufficiently low temperatures. We try then to fit physically reasonable functions to the experimental data below 300 K.

For the first polynomial coefficient a reasonable curve is the horizontal line $\Delta\tilde{C}_1 = 0$. The experimental data exhibit a progressive slight decrease up to 300 K; above 300 K this behavior is dramatically modified and $\Delta\tilde{C}_1$ decreases quite abruptly. For $\Delta\tilde{C}_2$ we used a Debye correlated model[3] with Debye temperature $\theta_D = 157$ K (solid line in Fig. 9); the experimental data were then vertically shifted to match the theoretical curve at 30 K. The model satisfactorily reproduces the slope of experimental data below 300 K, in agreement with the results obtained from the I L_3 EXAFS.[15,16] Above 300 K the experimental points progressively deviate to lower values with respect to the theoretical curve.

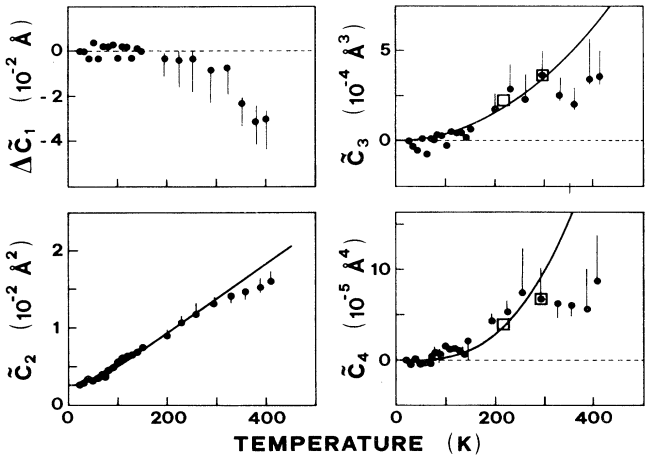

FIG. 9. Coefficients obtained from polynomial fits to EXAFS phases and amplitudes in the k ranges 8–16 and 5–16.5 Å^{-1}, respectively (solid circles). Solid lines are theoretical curves as explained in the text; the experimental values for $\tilde{C}_2$ have been vertically shifted to match the theoretical curve at 30 K. Vertical bars are mean-square deviations for different data reduction procedures. The squares in the $\tilde{C}_3$ and $\tilde{C}_4$ plots are results for CuBr (Ref. 7).

In their EXAFS study of CuBr, Tranquada and Ingalls showed that an anharmonic potential with the appropriate symmetry leads to a quadratic and cubic temperature dependence for the third and fourth cumulants, respectively.[7] If we tentatively assume a T^2 and T^3 behavior also for the third and fourth cumulants of AgI, a reasonable fit to experimental points is obtained below 300 K (solid lines in Fig. 9).

In conclusion, below 300 K all polynomial coefficients behave in agreement with physically reasonable models, while above 300 K they deviate in a more or less systematic way from the theoretical curves. The convergence interval of the cumulant series is expected to decrease when temperature increases. When we reduced the upper limit of the fitting range to 12 and 10.5 Å^{-1} for phases and amplitudes, respectively, the random spread of data increased, but the average trend was not modified. The anomalous behavior of the polynomial coefficients above 300 K cannot then be attributed to a reduction of the convergence interval of the cumulant series with respect to the EXAFS range.

Neglecting the third- and fourth-order terms in the analysis of phases and amplitudes, say, fitting the continuous curves in Figs. 7 and 8 by straight lines (standard analysis procedure), leads to an underestimate of interatomic distances and MSRD's. The introduction of higher-order terms (fifth and sixth) leads to a large random spread of values also for the lower-order coefficients.

V. TESTS ON MODEL DISTRIBUTIONS

To investigate the anomalous behavior of the polynomial coefficients above 300 K, we applied the same method of analysis utilized for experimental data to selected model distributions. This procedure allowed us to verify the correspondence between polynomial coefficients $\tilde{C}_i$ and exact cumulants C_i and the possibility of reproducing the distributions starting from the finite number of polynomial coefficients obtained from EXAFS.

The models utilized were (a),(b) two excluded-volume distributions convoluted with a Gaussian, with parameters best fitting the β-AgI EXAFS at 300 and 371 K, as reported by Hayes, Boyce, and Beeby;[14] (c) a skewed distribution $B\exp[-B(r-R_0)]$, with B =10, convoluted with a Gaussian of width σ =0.07 Å, considered also by Crozier, Rehr, and Ingalls;[8] (d) a Gaussian distribution of width σ =0.051 Å describing the situation in β-AgI at 23 K, assumed on the grounds of our results for $\tilde{C}_2$ (Fig. 9) and in agreement with the value 0.06 Å utilized by Boyce, Hayes, and Mikkelsen[13] at 77 K. These four distributions will be referred to as EV300, EV371, SK010, and GAU23, respectively; the first three are represented

by solid lines in Fig. 10. The corresponding effective distributions were calculated assuming a photoelectron mean free path $\lambda = 4$ Å.

The first six exact cumulants of the effective distributions EV300, EV371, and SK010 (Table I) were utilized to calculate approximate characteristic functions through Eq. (3) with the summation truncated at the sixth-order term. The characteristic functions (Fig. 11, left) were then Fourier transformed (the transform window for EV300 and EV371 is shown by dashed lines). The corresponding real distributions are shown by dotted lines in Fig. 10 (left). The difference between reconstructed and original distributions (P^r and P^0, respectively) was measured by the parameter

$$Q = \frac{1}{N} \sum_i \frac{|P_i^r - P_i^0|}{|P_i^0|},$$

where the summation refers to N equispaced points within the distance interval 2.6–3.15 Å. The Q values calculated for the three distributions were 5.1, 6.7, and 50, respectively. The poor reproduction of the SK010 distribution is not surprising, since its cumulant expansion diverges for $k > B/2$.[8] The EV300 and EV371 distributions are instead quite satisfactorily reproduced; the reduction of the significant k range in passing from EV300 to EV371 (Fig. 11, left) is probably due to the need of more than six cumulants rather than to nonconvergence. The different convergence properties of the EV300 and EV371 distributions with respect to SK010 can be understood in view of their different behavior for high r values prior to Gaussian broadening: While the exponentially skewed distribution is upward unlimited, the excluded-volume distributions for β-AgI are limited.

As a second step of the test procedure, an EXAFS function

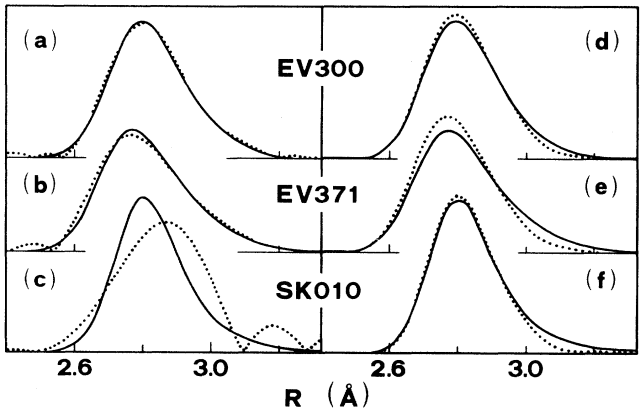

FIG. 10. Model distributions (solid lines): excluded-volume EV300 (a),(d) and EV371 (b),(e) and exponentially skewed SK010 (c),(f). Dotted lines are distributions reconstructed from the first six exact cumulants [left: (a),(b),(c)] and from polynomial coefficients of column (b) of Table I [right: (d),(e),(f)].

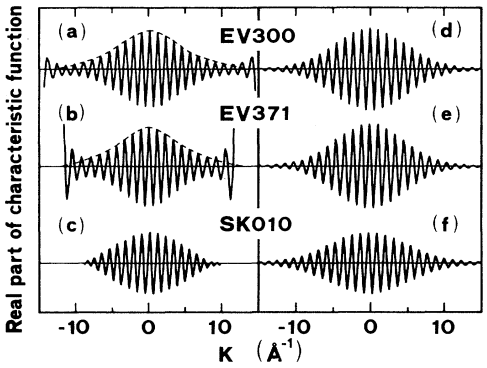

FIG. 11. Characteristic functions of the model distributions calculated through exact cumulants (left) and polynomial coefficients from EXAFS analysis (right). Column (b) of Table I was utilized; no significative differences were found when utilizing columns (a) or (c).

$$\int P(r,\lambda)\exp(2ikr)dr$$

was calculated for all the four model distributions. The EV300, EV371, and SK010 EXAFS were then analyzed utilizing GAU23 as reference and following exactly the same procedure utilized for the experimental data. The results of this analysis are summarized in Table I. The polynomial coefficients are always lower than the corresponding cumulants; the differences grow with growing asymmetry of the distribution (e.g., in passing from EV300 to EV371) and, in general, with growing cumulant order. No remarkable differences were found when the k range was shortened, in agreement with the results obtained for experimental data.

The deviations of the polynomial coefficients from the exact cumulants for the EV300 and EV371 model distributions are comparable with the deviations of the polynomial coefficients of experimental EXAFS data from the theoretical curves (solid circles and solid lines, respectively, in Fig. 9) at the corresponding temperatures. This result suggests that below 300 K the polynomial coefficients satisfactorily estimate the exact cumulants; above 300 K, with growing width and asymmetry of the distributions, the procedure of EXAFS analysis introduces a progressive reduction of the polynomial coefficients with respect to the exact cumulants. It seems, however, reasonable to recover the exact cumulants by extrapolating above 300 K the temperature dependence of the polynomial coefficients measured below 300 K by means of the theoretical curves shown as solid lines in Fig. 9.

As a further test, we utilized the polynomial coefficients obtained from EXAFS of the model distributions to reconstruct the characteristic functions (Fig. 11, right) and the corresponding distributions of distances (dotted lines in Fig. 10, right). In spite of the relatively large differences between polynomial coefficients and exact cumulants, the differences between reconstructed and original distributions are not dramatic (Table I).

The EXAFS signal corresponds to a finite portion of

TABLE I. Tests on excluded-volume (EV300 and EV371) and exponentially skewed (SK010) model distributions: first six cumulants of the effective distributions (calculated for λ=4 Å) and results of EXAFS analysis expressed as percent deviation of the polynomial coefficients with respect to exact cumulants. Phase and amplitude analyses were done up to both the (a) fourth- and (b) sixth-order polynomial coefficients with a k range extending to 16 $Å^{-1}$, and up to the (c) fourth order with a k range limited to 12 and 10.5 $Å^{-1}$ for phases and amplitudes, respectively. Q measures the difference between reconstructed and original distributions.

Distribution	Exact cumulants (effective distribution)	Polynomial coefficients from EXAFS (a)	(b)	(c)
EV300	C_1 = 2.8155	−0.6	−0.2	−0.6
	C_2 = 1.25×10^{-2}	−3.4	−16	−6.3
	C_3 = 6.75×10^{-4}	−58	−19	−55
	C_4 = 6.06×10^{-5}	−10	−110	−17
	C_5 = -5.15×10^{-6}		−149	
	C_6 = -3.81×10^{-6}		−66	
	Q =5.1	Q =24	Q =14	Q =19
EV371	C_1 = 2.8032	−1.1	−0.6	−1.1
	C_2 = 1.64×10^{-2}	−17	−30	−15
	C_3 = 1.35×10^{-3}	−77	−49	−75
	C_4 = 1.58×10^{-4}	−59	−108	−43
	C_5 = -3.89×10^{-6}		−190	
	C_6 = -1.31×10^{-5}		−87	
	Q =6.7	Q =26	Q =23	Q =26
SK010	C_1 = 2.8284	−0.8	−0.4	−0.8
	C_2 = 1.30×10^{-2}	−23	−30	−25
	C_3 = 1.45×10^{-3}	−86	−70	−33
	C_4 = 3.92×10^{-4}	−90	−98	−90
	C_5 = 1.42×10^{-4}		−98	
	C_6 = 6.46×10^{-5}		−101	
	Q =50	Q =24	Q =18	Q =23

the characteristic function; the procedure of analysis utilized in this work allows us to parametrize phase and amplitude of this portion in terms of polynomial coefficients, independently of the correspondence between polynomial coefficients and exact cumulants. The SK010 distribution is better reproduced starting from a limited portion of its characteristic function than from the exact cumulants, since the cumulant series has a very limited convergence interval. For the EV300 and EV371 distributions a worsening is noticed when using the polynomial coefficients from EXAFS analysis rather than the exact cumulants; this reflects the incomplete correspondence between polynomial coefficients and cumulants, which prevents an accurate reconstruction of the missing low-k part of the EXAFS signal. Actually the central parts of the characteristic functions are slightly higher in the right-hand than in the left-hand plots in Fig. 11. Correspondingly the high r tails of the real-space distributions are differently reproduced (Fig. 10).

Finally, the analysis of model distributions allowed us to test different choices in data analysis and to establish the optimized procedure which has been described in Sec. IV. The smallest discrepancies between polynomial coefficients and cumulants as well as the best reproduction of the original distributions were obtained when no sidelobes of the main peak were included in the Fourier back transform. Moreover, the phase differences between the EXAFS of the model distributions and of the GAU23 reference were characterized by a zero crossing at low k values as observed for the experimental data (Fig. 7); a shift ΔE_0 allowed us to eliminate or reduce the zero crossing but led to a poorer reproduction of both exact cumulants and original distributions.

VI. DISCUSSION

The cumulant analysis of β-AgI EXAFS was calibrated by the tests on model distributions. On these grounds we will now analyze the experimental results summarized in Fig. 9, first considering the possibility of reconstructing the distance distribution, and then studying the temperature dependence of each cumulant.

A. Distribution of distances

The experimental polynomial coefficients at 300 and 360 K have been utilized to calculate the approximate characteristic functions. In Fig. 12 the corresponding real distributions (dotted lines) are compared with the excluded-volume-model distributions EV300 and EV371 (solid lines). The agreement is much better at 300 K than at 360 K (Q=8.6 and 17, respectively). The reconstructed distributions mainly fail in reproducing the high-r tail; this failure reflects the defective reproduction

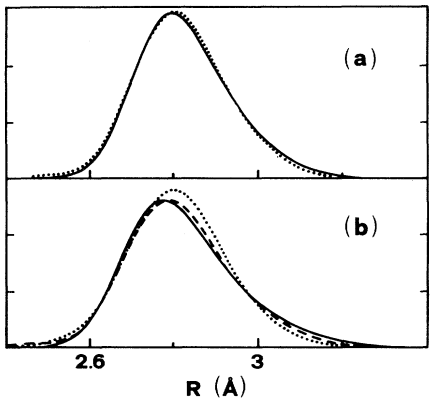

FIG. 12. Dotted lines are distributions of distances reconstructed from polynomial coefficients of β-AgI EXAFS at 300 K (a) and 360 K (b). Solid lines are excluded-volume distributions at 300 K (a) and 371 K (b). The dashed line in (b) was obtained by substituting the polynomial coefficients at 360 K (solid circles in Fig. 9) with the corresponding values on the theoretical curves (solid lines in Fig. 9).

of the low-k missing EXAFS due to the noncorrespondence between polynomial coefficients and exact cumulants.

The tests on model distributions suggested that the temperature dependence of cumulants above 300 K is satisfactorily approximated by the theoretical curves shown as solid lines in Fig. 9. We utilized then as cumulants the values given by these curves at 360 K: The corresponding distribution (dashed line in Fig. 12) is in satisfactory agreement with the excluded-volume model (Q=7.9) (the residual difference could be partly attributed to the 11-K temperature difference between model and experimental distributions).

The results obtained for β-AgI by the cumulant method are then consistent with those previously obtained by a real-space analysis based on the direct fit of the model to experimental distributions.[14] This agreement supports the hypothesis that the cumulants series for β-AgI is convergent within $k \leq 16.5$ Å^{-1} for temperatures as high as 360 K and that above 300 K the cumulants can be obtained by extrapolating their experimental behavior at lower temperatures.

B. Mean-square relative displacement

EXAFS analysis based on comparison with a reference gives only relative values ΔC_2 of the second cumulant. Below 300 K the slope of the experimental points of β-AgI is well reproduced by a Debye correlated model [Figs. 9 and 13(a)]. Absolute values of C_2 were obtained by vertically shifting the experimental points to match the model at low temperature. The relative discrepancy between cumulants of order higher than one of the effective and real distributions is proportional to C_2/C_1^2.[6] In the present case this relative discrepancy is about 0.001, negligible with respect to the overall experimental accuracy. We thus identify C_2 with the variance σ^2 of the real distribution, which measures the MSRD of the couple of absorber and backscatterer atoms.

The temperature dependence of the MSRD of the first-shell Ag–I distance obtained through the cumulant analysis of the Ag K EXAFS is in agreement with that previously obtained through a standard analysis of the I L_3 EXAFS for both β- and γ-AgI.[16] Elsewhere it was shown that also for the Ag K EXAFS a standard analysis limited to $k \leq 8$ Å^{-1} would give, below 300 K, the same temperature dependence of the MSRD.[24] In both cases (Ag K and I L_3 EXAFS) the temperature dependence of the MSRD is satisfactorily reproduced by a Debye correlated model[3,25] with the Debye temperature θ_D=157 K of the specific heat above 50 K.[11] Alternatively the Ag K data can be fitted by an Einstein model[26]

$$\sigma^2(T) = \frac{h}{8\pi^2 \mu \nu_E} \coth \frac{h\nu_E}{2kT},$$

where μ is the reduced mass of absorber and backscatterer atoms, and ν_E=2.77 THz [Fig. 13(b), solid line]. The I L_3 data were best fitted by a slightly lower frequency (2.65 THz). The Ag K and I L_3 results are in

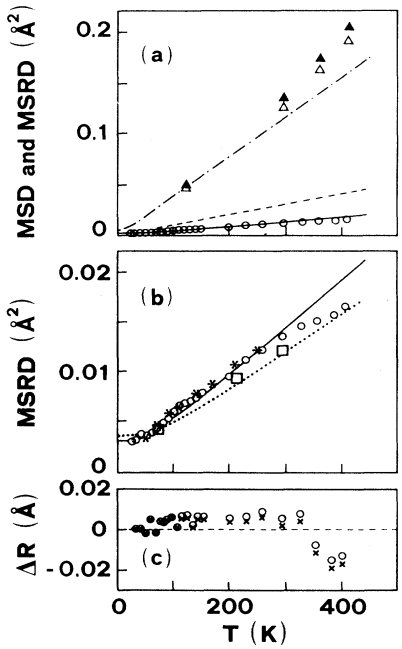

FIG. 13. (a) MSRD from Ag K EXAFS (open circles) compared with the sum of uncorrelated MSD's of silver and iodine obtained from XRD data through a harmonic (open triangles) and an anharmonic (solid triangles) refinement procedure (Ref. 12); solid and dotted lines represent correlated and uncorrelated Debye models, respectively; the dot-dashed line is an Einstein model. (b) β-AgI MSRD obtained from Ag K (circles) and I L_3 (asterisks) EXAFS compared with an Einstein model with 2.77 THz frequency (solid line); the dotted line is an Einstein model with 3.95 THz frequency and the squares are data for CuBr from Ref. 7, upward shifted to match the Einstein curve at 77 K. (c) Variation with temperature of the Ag–I distance calculated through Eq. (7), with λ=4 Å (circles) and λ= 12 Å (crosses).

agreement within the experimental uncertainty. In the following we will assume an average Einstein frequency ν_E=2.71±0.06 THz.

Despite the relatively strong anharmonicity of β-AgI, one cannot appreciate variations of the MSRD from the harmonic behavior below 300 K (above 300 K the artifacts of the data reduction procedure are not negligible). The quasiharmonic contribution to the MSRD has been evaluated to be negligible for AgI, owing to the very low average thermal expansion coefficient.

In their EXAFS study of anharmonicity in CuBr, Tranquada and Ingalls[7] obtained the MSRD and the higher-order cumulants by a data analysis similar to ours, although limited to three temperatures (71, 216, and 295 K at the Cu K edge). They found that the first-shell experimental relative $\Delta\sigma^2$ values were higher than those obtained from a shell-model calculation, while the Br-Br second-shell values agreed with the theoretical ones; they attributed this behavior to the anharmonic motion of Cu atoms. CuBr has the same zinc-blende structure of γ-AgI and similar lattice dynamical properties.[11] By applying the homology criterion for interatomic forces

$$\frac{\nu_{\mathrm{CuBr}}}{\nu_{\mathrm{AgI}}} = \left[\frac{(\mu a^2)_{\mathrm{AgI}}}{(\mu a^2)_{\mathrm{CuBr}}}\right]^{\frac{1}{2}},$$

where a are the lattice constants[27] and ν_{AgI}=2.71 THz, we found a frequency ν_{CuBr}=3.95±0.09 THz. The slope of experimental data reported for CuBr by Tranquada and Ingalls is consistent with this harmonic behavior [Fig. 13(b), dotted line]. Actually one should be very cautious in calculating the harmonic contribution to MSRD from theoretical models; the MSRD is sensitive to correlation of atomic motion and it is well established that different vibrational dynamics models, though giving the same dispersion curves, can yield different eigenvectors.[29,30]

The MSRD sampled by EXAFS contains the contribution from the mean-square displacements (MSD's) of absorber and backscatterer atoms and the displacement correlation function (DCF).[3,15] Yoshiasa *et al.* made single-crystal XRD measurements on β-AgI at four temperatures (123, 297, 363, and 413 K) and obtained the second-order anisotropic temperature coefficients β_{ij} through both a purely harmonic refinement procedure and a procedure allowing for cumulants up to the fourth order.[12] From the temperature coefficients β_{ij} we calculated the MSD's of iodine and silver, which are with good approximation independent of direction for both atoms. We can then refer to the radial MSD,[28]

$$\langle u^2\rangle_r = \frac{1}{6\pi^2}\left(\frac{3}{2}a^2\beta_{11} + c^2\beta_{33}\right),$$

where a and c are the lattice constants of β-AgI in the wurtzite structure. The contribution to the Ag-I MSRD from uncorrelated atomic motion, sum of the MSD's of silver and iodine, is shown in Fig. 13(a) as a function of temperature. The values obtained through a purely harmonic analysis (open triangles) are lower than those obtained through a cumulant analysis (solid triangles). In the following we will refer only to the results of XRD cumulant analysis. The MSRD's obtained from EXAFS analysis are also shown in Fig. 13(a). The large difference in slope between XRD and EXAFS results is due to a strong influence of the correlation of atomic motion, and has been discussed elsewhere.[15]

A rough estimate of the influence of anharmonicity on the uncorrelated MSD's has been attempted by considering a harmonic model fitting the experimental value at 123 K. The difference between experimental MSD values and harmonic model grows with temperature and is 12% at 300 K and 22% at 413 K. A comparable influence of anharmonicity on the EXAFS MSRD seems incompatible with our experimental data, which are reasonably fitted by an harmonic model up to 300 K. Above 300 K the difference between experimental points and the harmonic curve is accounted for by the artifacts of data reduction. It is reasonable to assume that even above 300 K the deviation from harmonic behavior is smaller for the EXAFS MSRD than for the XRD MSD's. This result can be physically explained by considering that the spread of interatomic distances is smaller than the spread of atomic positions because of correlation effects. Harmonic approximation is more valid for narrower distributions.

C. Interatomic distance

The difference between average values of real and effective distributions, Eq. (7), requires the knowledge of C_2 and λ. The determination of the photoelectron mean free path λ is not trivial. Theoretical calculations based on a complex Hedin-Lundqvist potential led to a value $\lambda \simeq 4$ Å for β-AgI.[23] An experimental evaluation of the mean free path was done for the tetrahedral semiconductors GaAs, ZnSe, and CuBr by Stern, Bunker, and Heald;[31] those authors found a systematic increasing of λ with ionicity; since the Phillips ionicity of AgI (0.770) is comparable to that of CuBr (0.735), we can assume that also the mean free paths are similar. The λ values plotted versus k for CuBr by Stern, Bunker, and Heald do not exceed the value of 12 Å. In Fig. 13(c) the variation with temperature of the real interatomic distance calculated through Eq. (7) is shown for λ=4 and 12 Å. The difference between the two cases is almost negligible with respect to the spread of experimental points. Tranquada and Ingalls in their EXAFS work on CuBr considered a mean free path λ=8 Å.[7]

XRD measurements by Yoshiasa *et al.*[12] show that both the basal and apical Ag–I distances do not vary with temperature by more than 0.02 Å and the average distance, to be compared with EXAFS results, is constant to within 0.002 Å. The spread of values of distance obtained from EXAFS below 300 K, which measures the experimental uncertainty, is of the order of 0.01 Å.

D. Higher-order cumulants

The cumulants C_3 and C_4 of the effective distribution can be identified as the cumulants of the real distribu-

tion, since the relative discrepancies are negligible. The third- and fourth-order cumulants measure the deviation of the distribution from a Gaussian shape. The third cumulant reflects the degree of asymmetry of the distribution; its positive value is connected with the presence of a tail on the high-r side of the distribution. The positive value of the fourth cumulant indicates a distribution narrower at the center and broader at the borders than a Gaussian one. The values obtained for AgI in this work are very similar to those quoted for CuBr by Tranquada and Ingalls[7] (open squares in Fig. 9).

In β-AgI silver ions are coordinated to four iodine ions forming a tetrahedron, which is anisotropically deformed with temperature. Our EXAFS analysis was done assuming a Gaussian distribution for β-AgI at 23 K. We can now investigate the reliability of this hypothesis. No crystallographic data are available at 23 K. We can, however, refer to XRD measurements of Yoshiasa *et al.*[12] At 123 K the tetrahedron of iodine atoms surrounding each silver atom is slightly distorted, the apical distance being 0.008 Å longer than the three basal distances. When the temperature increases, the tetrahedron is compressed along the c axis and the apical distance becomes shorter than the basal distance. The first four cumulants of the distribution of distances in the distorted tetrahedron measured by Yoshiasa *et al.* at 23 K are $C_1 = 2.813$ Å, $C_2 = 1.2 \times 10^{-5}$ Å^2, $C_3 = 4.8 \times 10^{-7}$ Å^3, and $C_4 = -9.6 \times 10^{-11}$ Å^4. These values for the second, third, and fourth cumulants are much lower than the statistical fluctuations of the values obtained by our EXAFS analysis (Fig. 9). We can conclude that the static disorder due to the deformation of the AgI_4 tetrahedron is below the sensitivity threshold of EXAFS; this *a posteriori* justifies the choice of the 23-K EXAFS as reference compound.

VII. CONCLUSIONS

This work has led to specific results on the local structure and dynamics of β-AgI and more general results concerning strengths and limitations of the cumulant expansion of EXAFS.

The cumulant analysis qualitatively monitors the progressive deviation of the Ag–I distance distribution from a Gaussian shape with growing temperature. Standard analysis, based on the approximation of small Gaussian disorder, would produce large errors in the determination of physical parameters at high temperatures.

A reliable quantitative analysis is possible only if the cumulant series rapidly converges within the EXAFS range. The polynomial coefficients from EXAFS analysis then correspond to cumulants, and their knowledge allows one to recover the low-k missing signal. For β-AgI the comparison between experimental data and the physically consistent excluded-volume model[14] shows that the whole k range from 2.5 to 16.5 Å^{-1} can be utilized for cumulant analysis at least up to 360 K. The progressive deviation of polynomial coefficients from cumulants above 300 K is due to artifacts of the data reduction procedure; the cumulants can be recovered above 300 K by extrapolating their low-temperature behavior.

The results obtained for β-AgI cannot easily be generalized. One can anyway expect that the cumulant method is more appropriate for systems in which the distribution of distances is upper limited than for systems in which it has no upper limit. As a matter of fact, distributions of similar shape, such as the excluded-volume and exponentially skewed distributions, can be characterized by very different convergence properties of the cumulant series. The results for AgI suggest that the reliability of cumulant analysis could be roughly estimated from the physical consistency of the temperature dependence of the polynomial coefficients. Further work on different systems would be useful to clarify this point.

The distributions of distances reconstructed from cumulants at 300 and 360 K are consistent with those calculated by the excluded-volume model.[14] This model is appealing for its ability to account for the superionic transition in a simple way. It is, however, based on a rather crude approximation of the interatomic potential. Besides, it does not allow the separation of static and thermal disorder. More refined model-independent information on the interatomic potentials can in principle be gained from cumulant analysis of EXAFS.[7] A complete investigation of this subject was beyond the aims of this work. Some partial conclusions can anyway be drawn for what concerns the MSRD.

The strong anharmonicity of β-AgI is monitored by the growth with temperature of the third- and fourth-order cumulants. Also the uncorrelated mean-square displacements (MSD's) of silver and iodine atoms measured by XRD are strongly affected by anharmonicity.[12] The mean-square relative displacement (MSRD) of the Ag–I distance measured by EXAFS can instead be satisfactorily fitted by harmonic models. The difference between XRD MSD and EXAFS MSRD is due to the strong correlation of motion of nearest-neighbor atoms,[15] which greatly narrows the Ag–I distance distribution. As a consequence, the MSRD mainly depends on the harmonic part of the potential and can be properly checked against harmonic vibrational dynamics models.

ACKNOWLEDGMENTS

The authors are grateful to P. Maistrelli, A. Sadoc, and the technical staff of LURE laboratories for collaboration in EXAFS measurements. This work has been partially supported by Consiglio Nazionale delle Ricerche Grant No. 90.00113.CT02.

[1]F. W. Lytle, D. E. Sayers, and E. A. Stern, Phys. Rev. B **11**, 4825 (1975).
[2]P. A. Lee, P. H. Citrin, P. Eisenberger, and B. M. Kincaid, Rev. Mod. Phys. **53**, 769 (1981).
[3]G. Beni and P. M. Platzman, Phys. Rev. B **14**, 1514 (1976).
[4]P. Eisenberger and G. S. Brown, Solid State Commun. **29**, 481 (1979).
[5]E. D. Crozier and A. J. Seary, Can. J. Phys. **58**, 1388 (1980).
[6]G. Bunker, Nucl. Instrum. Methods **207**, 437 (1983).
[7]J. M. Tranquada and R. Ingalls, Phys. Rev. B **28**, 3520

(1983).
[8]E. D. Crozier, J. J. Rehr, and R. Ingalls, in *X-Ray Absorption*, edited by D. C. Koningsberger and R. Prins (Wiley, New York, 1988).
[9]P. R. Prager, Prog. Cryst. Growth Char. **7**, 451 (1983).
[10]R. J. Cava, F. Reidinger, and B. J. Wuensch, Solid State Commun. **24**, 411 (1977).
[11]W. Bührer, R. M. Nicklow, and P. Brüesch, Phys. Rev. B **17**, 3362 (1978).
[12]A. Yoshiasa, K. Koto, F. Kanamaru, S. Emura, and H. Horiuchi, Acta Crystallogr. B **43**, 434 (1987).
[13]J. B. Boyce, T. M. Hayes, and J. C. Mikkelsen, Jr., Phys. Rev. B **23**, 2876 (1981).
[14]T. M. Hayes, J. B. Boyce, and J. L. Beeby, J. Phys. C **11**, 2931 (1978).
[15]G. Dalba, P. Fornasini, F. Rocca, and S. Mobilio, Phys. Rev. B **41**, 9668 (1990).
[16]G. Dalba, P. Fornasini, and F. Rocca, J. Phys. C **4**, 1121 (1992).
[17]G. Dalba, P. Fornasini, F. Rocca, and A. Sadoc, J. Phys. (Paris) Colloq. **53**, C2-207 (1992).
[18]B. V. Gnedenko, *The Theory of Probability* (MIR, Moscow, 1976).
[19]H. Cramér, *Mathematical Methods of Statistics* (Princeton University Press, Princeton, 1966).
[20]S. M. Angeretti, G. Dalba, P. Fornasini, M. Benfatto, and F. Rocca, Phys. Rev. B **44**, 11569 (1991).
[21]B. Lengeler and P. Eisenberger, Phys. Rev. B **21**, 4507 (1980).
[22]P. A. Lee and G. Beni, Phys. Rev. B **15**, 2862 (1977).
[23]S. M. Angeretti (private communication).
[24]G. Dalba, D. Diop, P. Fornasini, P. Maistrelli, and F. Rocca, in *X-ray Absorption Fine Structure*, edited by S. S. Hasnain (Horwood, Chichester, 1991), p. 409.
[25]W. Böhmer and P. Rabe, J. Phys. C **12**, 2465 (1979).
[26]E. Sevillano, H. Meuth, and J. J. Rehr, Phys. Rev. B **20**, 4908 (1979).
[27]R. W. G. Wyckoff, *Crystal Structures* (Wiley, New York, 1963).
[28]B. T. M. Willis and A. W. Pryor, *Thermal Vibrations in Crystallography* (Cambridge University Press, Cambridge, England, 1975).
[29]R. S. Leigh, B. Szigeti, and V. K. Tewary, Proc. R. Soc. London A **320**, 505 (1971).
[30]W. Cochran, Acta Crystallogr. A **27**, 556 (1971).
[31]E. A. Stern, B. A. Bunker, and S. M. Heald, Phys. Rev. B **21**, 5521 (1980).